Mössbauer and EPR Characterization of the $S = {}^9/_2$ Mixed-Valence Fe(II)Fe(III) Cluster in the Cryoreduced R2 Subunit of *Escherichia coli* Ribonucleotide Reductase

Carsten Krebs,[†] Roman Davydov,[§] Jeff Baldwin,[‡] Brian M. Hoffman,[§] J. Martin Bollinger, Jr.,[‡] and Boi Hanh Huynh*[,†]

Contributions from the Department of Physics, Rollins Research Center, Emory University, Atlanta, Georgia 30322, Department of Chemistry, Northwestern University, Evanston, Illinois 60208, and Departments of Biochemistry and Molecular Biology, Pennsylvania State University, University Park, Pennsylvania 16802

Received January 28, 2000

Abstract: Low-temperature (77 K) radiolytic reduction of the diferric cluster in the met R2 subunit of *Escherichia coli* ribonucleotide reductase yields an antiferromagnetically coupled mixed-valence Fe(II)Fe(III) cluster ($[R2_{met}]_{mv1/2}$). Annealing the radiolytically reduced sample at 180 K converts the mixed-valence cluster in $[R2_{met}]_{mv1/2}$ into a ferromagnetically coupled cluster having an $S = {}^9/_2$ ground state ($R2_{mv9/2}$). We have used Mössbauer and EPR spectroscopy to study the electronic and magnetic properties of $R2_{mv9/2}$. The Mössbauer data, recorded over wide ranges of temperature and applied field, indicate that the mixed-valence cluster in $R2_{mv9/2}$ is valence localized. The spectra can be deconvoluted into two spectral components, of which analysis yields parameters ($\delta = 1.25$ mm/s, $\Delta E_Q = -2.80$ mm/s, $\eta = 1.30$, and $\mathbf{a}/g_n\beta_n = -(13.5, 10.8, 20.3)$ T for site 1; and $\delta = 0.53$ mm/s, $\Delta E_Q = -0.57$ mm/s, $\eta = -3$, and $\mathbf{a}/g_n\beta_n = -(22.1, 22.0, 22.0)$ T for site 2) that are characteristic of high-spin ferrous (site 1) and high-spin ferric (site 2) ions with octahedral O/N coordination. The spin−spin interaction between the two valence localized iron sites is ferromagnetic and the effective exchange coupling constant (J_{eff} in the exchange Hamiltonian $J_{eff}\mathbf{S}_1\cdot\mathbf{S}_2$) is estimated to be ca. -12 cm^{-1} from the high-temperature strong-field data. Taking into consideration the various factors that control the electronic properties of a mixed-valence Fe(II)Fe(III) compound and comparing the observed spectroscopic properties of $R2_{mv9/2}$ with those of model complexes, a core structure with two single-oxygen bridges is proposed for $R2_{mv9/2}$. It is suggested that conversion of $[R2_{met}]_{mv1/2}$ to $R2_{mv9/2}$ may involve a carboxylate shift of E238 from a monodentate terminal chelating mode to a monodentate bridging and chelating mode, in addition to protonation of the oxo bridge. $R2_{mv9/2}$ displays EPR signals at $g = 14-15$, 6.6, and 5.4. Analysis of the data indicates that these features can be properly simulated by assuming an $S = {}^9/_2$ center with a central E/D of 0.05 and a distribution in E/D ($\sigma_{E/D} = 0.023$). Effects of E/D distribution on the EPR spectrum are discussed.

Introduction

Ribonucleotide reductases (RNRs) catalyze the reduction of ribonucleotides to the corresponding deoxyribonucleotides, the rate-limiting step in DNA biosynthesis. According to their cofactor compositions, RNRs may be divided into four classes.[1,2] Aerobic RNR from *E. Coli* belongs to class I, and comprises two homodimeric subunits, R1 (2 × 86 kD) and R2 (2 × 43 kD). The R1 subunit contains redox active cysteines for substrate reduction, and binding sites for substrate and allosteric effectors. The active form of the R2 subunit, $R2_{act}$, harbors a catalytically essential tyrosyl radical located at residue 122, in close proximity to a carboxylate bridged μ-oxo diferric cluster.[3−5] The diiron cluster-Y122$^\bullet$ cofactor in $R2_{act}$ can be generated by reacting apo R2 with ferrous ions and O_2.[6] The mechanism of this cofactor assembly has been the subject of extensive investigations.[7−13]

The tyrosyl radical of $R2_{act}$ can be reduced chemically leaving the diiron cluster in the diferric form ($R2_{met}$). The structure of the diferric cluster in $R2_{met}$ has been determined by X-ray crystallography[4,5] and is similar to other carboxylate-bridged diiron clusters found in various proteins, including the soluble methane monooxygenase,[14−16] stearoyl-acyl carrier protein Δ^9

* Address correspondence to this author.
[†] Emory University.
[§] Northwestern University.
[‡] Pennsylvania State University.

(1) Reichard, P. *Science (Washington, D.C.)* **1993**, *260*, 1773−1777.
(2) Stubbe, J.; van der Donk, W. A. *Chem. Rev. (Washington, D.C.)* **1998**, *98*, 705−762.
(3) Sahlin, M.; Petersson, L.; Gräslund, A.; Ehrenberg, A.; Sjöberg, B. M.; Thelander, L. *Biochemistry* **1987**, *26*, 5541−5548.
(4) Nordlund, P.; Eklund, H. *J. Mol. Biol.* **1993**, *232*, 123−164.
(5) Nordlund, P.; Sjöberg, B. M.; Eklund, H. *Nature (London)* **1990**, *345*, 593−598.
(6) Atkin, C. L.; Thelander, L.; Reichard, P.; Lang, G. *J. Biol. Chem.* **1973**, *248*, 7464−7472.
(7) Bollinger, J. M., Jr.; Tong, W. H.; Ravi, N.; Huynh, B. H.; Edmondson, D. E.; Stubbe, J. *J. Am. Chem. Soc.* **1994**, *116*, 8015−8023.
(8) Ravi, N.; Bollinger, J. M., Jr.; Huynh, B. H.; Stubbe, J.; Edmondson, D. E. *J. Am. Chem. Soc.* **1994**, *116*, 8007−8014.
(9) Parkin, S. E.; Chen, S.; Ley, B. A.; Mangravite, L.; Edmondson, D. E.; Huynh, B. H.; Bollinger, J. M., Jr. *Biochemistry* **1998**, *37*, 1124−1130.
(10) Bollinger, J. M., Jr.; Stubbe, J.; Huynh, B. H.; Edmondson, D. E. *J. Am. Chem. Soc.* **1991**, *113*, 6289−6291.
(11) Ochiai, E.; Mann, G. J.; Gräslund, A.; Thelander, L. *J. Biol. Chem.* **1990**, *265*, 15758−15761.
(12) Krebs, C.; Huynh, B. H. In *Iron Metabolism: Inorganic Biochemistry and Regulatory Mechanisms*; Ferreira, G. C., Moura, J. J. G., Franco, R., Eds.; Wiley-VCH: Weinheim, Germany, 1999; pp 253−273.
(13) Fontecave, M.; Eliasson, R.; Reichard, P. *J. Biol. Chem.* **1989**, *264*, 9164−9170.
(14) Rosenzweig, A. C.; Frederick, C. A.; Lippard, S. J.; Nordlund, P. *Nature (London)* **1993**, *366*, 537−543.

10.1021/ja000317z CCC: $19.00
Published on Web 05/20/2000

desaturase,[17] hemerythrin,[18] purple acid phosphatases,[19] and ferritin.[20−24] It has been shown that $R2_{met}$ can be reduced by one electron to a mixed-valence Fe(II)Fe(III) state ($[R2_{met}]_{mv}$) by low-temperature radiolysis.[25−28] The initial $[R2_{met}]_{mv}$ generated at low temperature (77 K), termed $[R2_{met}]_{mv1/2}$, exhibits EPR signals at $\mathbf{g} < 2$ ($g_\perp = 1.936$ and $g_\parallel = 1.818$)[26−28] typical of an antiferromagnetically coupled mixed-valence Fe(II)Fe(III) cluster with an $S = {}^1/_2$ ground state. This result has been explained[26] by the fact that $[R2_{met}]_{mv1/2}$ generated at low temperature is trapped in the equilibrium geometry of the oxidized Fe(III)Fe(III) cluster in $R2_{met}$, in which the two ferric ions are antiferromagnetically coupled via an oxo bridge.[6,29] Annealing the irradiated sample at temperatures higher than 160 K converts $[R2_{met}]_{mv1/2}$ into a species with an $S = {}^9/_2$ ground state, designated $R2_{mv9/2}$, which displays EPR signals at $g \sim 14-15$, 6.6, and 5.4.[25−27] The signal at $g \sim 14-15$ was attributed to the lowest Kramers doublet of the $S = {}^9/_2$ state and the signals at $g = 6.6$ and 5.4 to the excited doublet. These observations reveal that an interesting structural change is taking place at temperatures above 160 K, and causes a switch of the electronic ground state of $[R2_{met}]_{mv}$ from $S = {}^1/_2$ to ${}^9/_2$. Protonation of the oxo bridge has been suggested as a possible cause for this switch.[26] Annealing at temperatures higher than 230 K results in an EPR silent state suggesting that $R2_{mv9/2}$ is unstable with respect to disproportionation.[26] The presence of $Y122^\bullet$ and the mutation of Y122F have been shown to affect noticeably the EPR properties of the initially generated cryoreduced mixed-valence $S = {}^1/_2$ species, indicating that the structure of the diiron site is sensitive to the nature of the Y122 site.[27]

Mixed-valence Fe(II)Fe(III) compounds have attracted the interest of many bioinorganic investigators. This is because polynuclear iron clusters are prevalent in metalloproteins, and binuclear iron clusters represent the simplest unit for studying metal−metal interactions within an Fe cluster. In particular, the mixed-valence state is paramagnetic, making it accessible for detailed investigation by a variety of spectroscopic techniques. The electronic and magnetic properties of a mixed-valence Fe(II)Fe(III) cluster with d^6-d^5 high-spin configuration are results of a sensitive interplay of the following factors: (1) the Heisenberg Dirac van Vleck (HDvV) exchange interaction, (2) double exchange interaction, (3) vibronic coupling, and (4) the asymmetry of the ligand environments of the two iron sites.[30] In general, the HDvV exchange interaction dominates in a μ-oxo, μ-hydroxo, or μ-sulfido binuclear Fe(II)Fe(III) cluster, resulting in the $S = {}^1/_2$ ground state observed for the majority of model compounds and proteins. The $S = {}^9/_2$ ground state is less common, although it has been observed for several model compounds[31−34] and site-specific mutants of a 2Fe-2S ferredoxin.[35−37] Protein R2 is the only wild-type protein that affords an $S = {}^9/_2$ ground state for its diiron cluster in the mixed-valence form. To provide better insight into the electronic properties of this interesting complex, we have applied Mössbauer spectroscopy to investigate a low-temperature γ-irradiated $R2_{met}$ sample that has been annealed at 180 K. The results reveal a valence localized $R2_{mv9/2}$, suggesting that double exchange may not be the dominating factor for stabilization of the $S = {}^9/_2$ ground state but that other factors are also important in determining the electronic properties of $R2_{mv9/2}$. We have also studied this $R2_{mv9/2}$ state using EPR spectroscopy. It has been noted previously that the EPR features at $g = 6.6$ and 5.4 are not predicted by a simplistic description of an $S = {}^9/_2$ center.[25] We found that these features can be properly simulated by assuming an $S = {}^9/_2$ center with a distribution in the zero-field splitting parameter E/D. Effects of E/D distribution on the EPR spectrum are presented and discussed.

Methods

Sample Preparation. $R2_{met}$ in a 1:1 (v/v) mixture of buffer and glycerol was prepared as described in the literature.[26] Irradiation of the samples was carried out at 77 K using a ^{60}Co source. The low-temperature irradiated samples were annealed at 180 K for ~4 min in a liquid-nitrogen chilled isopentane bath.

Spectroscopic Measurements. Mössbauer spectra were recorded in either a weak-field spectrometer equipped with a Janis 8DT variable-temperature cryostat or a strong-field spectrometer furnished with a Janis CNDT/SC SuperVaritemp cryostat encasing an 8-T superconducting magnet. Both spectrometers operate in a constant acceleration mode in a transmission geometry. The zero velocity of the spectra refers to the centroid of a room-temperature spectrum of a metallic iron foil. EPR spectra were recorded in a Bruker ER-200D-SRC spectrometer equipped with an Oxford Instruments ESR 910 continuous-flow cryostat.

Spectral Analysis. In analyzing the low-temperature Mössbauer and EPR spectra of the mixed-valence Fe(II)Fe(III) cluster in $R2_{mv9/2}$, the following spin Hamiltonian (H_S) was used to describe the electronic properties of the ground $S = {}^9/_2$ state and the hyperfine interactions of the two iron nuclei with their surrounding electrons.

$$H_S = H_e + H_{hf} \quad (1)$$

(15) Rosenzweig, A. C.; Nordlund, P.; Takahara, P. M.; Frederick, C. A.; Lippard, S. J. *Chem. Biol.* **1995**, *2*, 409−418.
(16) Elango, N.; Radhakrishnan, R.; Froland, W. A.; Wallar, B. J.; Earhart, C. A.; Lipscomb, J. D.; Ohlendorf, D. H. *Protein Sci.* **1997**, *6*, 556−568.
(17) Fox, B. G.; Shanklin, J.; Somerville, C.; Münck, E. *Proc. Natl. Acad. Sci. U.S.A.* **1993**, *90*, 2486−2490.
(18) Stenkamp, R. E.; Sieker, L. C.; Jensen, L. H. *J. Am. Chem. Soc.* **1984**, *106*, 618−622.
(19) Sträter, N.; Klabunde, T.; Tucker, P.; Witzel, H.; Krebs, B. *Science* **1995**, *268*, 1489−1492.
(20) Hempstead, P. D.; Yewdall, S. J.; Fernie, A. R.; Lawson, D. M.; Artymiuk, P. J.; Rice, D. W.; Ford, G. C.; Harrison, P. M. *J. Mol. Biol.* **1997**, *268*, 424−448.
(21) Moënne-Loccoz, P.; Krebs, C.; Herlihy, K.; Edmondson, D. E.; Theil, E. C.; Huynh, B. H.; Loehr, T. M. *Biochemistry* **1999**, *38*, 5290−5295.
(22) Pereira, A. S.; Tavares, P.; Krebs, C.; Huynh, B. H.; Rusnak, F.; Moura, I.; Moura, J. J. G. *Biochem. Biophys. Res. Commun.* **1999**, *260*, 209−215.
(23) Ha, Y.; Shi, D.; Small, G. W.; Theil, E. C.; Allewell, N. M. *J. Biol. Inorg. Chem.* **1999**, *4*, 243−256.
(24) Hwang, J.; Krebs, C.; Huynh, B. H.; Edmondson, D. E.; Theil, E. C.; Penner-Hahn, J. E. *Science (Washington, D.C.)* **2000**, *287*, 122−125.
(25) Hendrich, M. P.; Elgren, T. E.; Que, L., Jr. *Biochem. Biophys. Res. Commun.* **1991**, *176*, 705−710.
(26) Davydov, R.; Kuprin, S.; Gräslund, A.; Ehrenberg, A. *J. Am. Chem. Soc.* **1994**, *116*, 11120−11128.
(27) Davydov, R.; Sahlin, M.; Kuprin, S.; Gräslund, A.; Ehrenberg, A. *Biochemistry* **1996**, *35*, 5571−5576.
(28) Davydov, R. M.; Davydov, A.; Ingemarson, R.; Thelander, L.; Ehrenberg, A.; Gräslund, A. *Biochemistry* **1997**, *36*, 9093−9100.
(29) Petersson, L.; Gräslund, A.; Ehrenberg, A.; Sjöberg, B. M.; Reichard, P. *J. Biol. Chem.* **1980**, *255*, 6706−6712.
(30) Blondin, G.; Girerd, J. J. *Chem. Rev.* **1990**, *90*, 1359−1376.
(31) Surerus, K. K.; Münck, E.; Snyder, B. S.; Holm, R. H. *J. Am. Chem. Soc.* **1989**, *111*, 5501−5502.
(32) Ding, X. Q.; Bominaar, L.; Bill, E.; Winkler, H.; Trautwein, A. X.; Drüeke, S.; Chaudhuri, P.; Wieghardt, K. *J. Chem. Phys.* **1990**, *92*, 178−186.
(33) Saal, C.; Mohanta, S.; Nag, K.; Dutta, S. K.; Werner, R.; Haase, W.; Duin, E.; Johnson, M. K. *Ber. Bunsen-Ges.* **1996**, *100*, 2086−2090.
(34) Hagadorn, J. R.; Que, L., Jr.; Tolman, W. B.; Prisecaru, I.; Münck, E. *J. Am. Chem. Soc.* **1999**, *121*, 9760−9761.
(35) Crouse, B. R.; Meyer, J.; Johnson, M. K. *J. Am. Chem. Soc.* **1995**, *117*, 9612−13.
(36) Achim, C.; Golinelli, M.-P.; Bominaar, E. L.; Meyer, J.; Münck, E. *J. Am. Chem. Soc.* **1996**, *118*, 8168−8169.
(37) Achim, C.; Bominaar, E. L.; Meyer, J.; Peterson, J.; Münck, E. *J. Am. Chem. Soc.* **1999**, *121*, 3704−3714.

where H_e describes the energy levels of the $S = {}^9/_2$ multiplet

$$H_e = D\left[\mathbf{S}_z^2 - \frac{S(S+1)}{3} + \frac{E}{D}(\mathbf{S}_x^2 - \mathbf{S}_y^2)\right] + \beta\mathbf{S}\cdot\mathbf{g}\cdot\mathbf{H} \qquad (2)$$

and H_{hf} describes the hyperfine interactions

$$H_{hf} = \sum_{i=1}^{2}\frac{eQ(V_{zz})_i}{4}\left[\mathbf{I}_{zi}^2 - \frac{I_i(I_i+1)}{3} + \frac{\eta}{3}(\mathbf{I}_{xi}^2 - \mathbf{I}_{yi}^2)\right] + \sum_{i=1}^{2}(\mathbf{S}\cdot\mathbf{A}_i\cdot\mathbf{I}_i - g_n\beta_n\mathbf{H}\cdot\mathbf{I}_i) \qquad (3)$$

For analysis of the high-temperature Mössbauer data, the excited spin multiplets need to be considered, and the Hamiltonian H_e used to describe the electronic part of the spin Hamiltonian can be rewritten as

$$H_e = J_{eff}\mathbf{S}_1\cdot\mathbf{S}_2 + \sum_{i=1}^{2}D_i\left[\mathbf{S}_{zi}^2 - \frac{S(S+1)}{3} + \frac{E_i}{D_i}(\mathbf{S}_{xi}^2 - \mathbf{S}_{yi}^2)\right] + \sum_{i=1}^{2}\beta\mathbf{S}_i\cdot\mathbf{g}_i\cdot\mathbf{H} \qquad (4)$$

where $S_1 = 2$ and $S_2 = {}^5/_2$ are the intrinsic spins of the ferrous and ferric sites, respectively. The intrinsic zero-field splitting parameters D_1 and D_2 for the ferrous and ferric sites, respectively, are related to the zero-field splitting parameter of the $S = {}^9/_2$ ground state by[38]

$$D = \frac{3}{18}D_1 + \frac{5}{18}D_2 \qquad (5)$$

In general, the zero-field splitting parameters of ferric sites are smaller than that of ferrous sites. For simplicity, we have assumed $D_2 = 0$ and defined $D_1 = 6D$. The hyperfine interactions are expressed as

$$H_{hf} = \sum_{i=1}^{2}\frac{eQ(V_{zz})_i}{4}\left[\mathbf{I}_{zi}^2 - \frac{I_i(I_i+1)}{3} + \frac{\eta}{3}(\mathbf{I}_{xi}^2 - \mathbf{I}_{yi}^2)\right] + \sum_{i=1}^{2}(\mathbf{S}_i\cdot\mathbf{a}_i\cdot\mathbf{I}_i - g_n\beta_n\mathbf{H}\cdot\mathbf{I}_i) \qquad (6)$$

where $\mathbf{a}_1$ and $\mathbf{a}_2$ are the intrinsic magnetic hyperfine coupling tensors for the ferrous and ferric sites, respectively. They are related to the effective **A** tensors of eq 3 by the following equations.

$$\mathbf{A}_1 = \frac{4}{9}\mathbf{a}_1; \qquad \mathbf{A}_2 = \frac{5}{9}\mathbf{a}_2 \qquad (7)$$

Analysis of the low-temperature spectra in terms of an isolated $S = {}^9/_2$ multiplet is valid for $|J| \gg |D_i|$. With the J value determined for $R2_{mv9/2}$ (see Results), this condition does not strictly hold. We have therefore checked the validity of our approach by comparing spectra simulated with and without the excited spin states (i.e., eq 4 vs eq 2). We found that the spectra are only slightly perturbed by the relatively low-lying $S = {}^7/_2$ multiplet.

Mössbauer spectra were simulated using the program WMOSS (WEB Research), and EPR spectra were simulated using the program by Gaffney and Silverstone,[39] which has been modified for $S = {}^9/_2$.[40] For simulations assuming a distribution in the rhombicity E/D, spectra were calculated for various values of E/D (the step width was 0.001 and 0.005 for the EPR and Mössbauer simulations, respectively) and added together according to the probability factor from a Gaussian distribution with a standard deviation $\sigma_{E/D}$. Contributions of E/D within 6 $\sigma_{E/D}$ were considered.

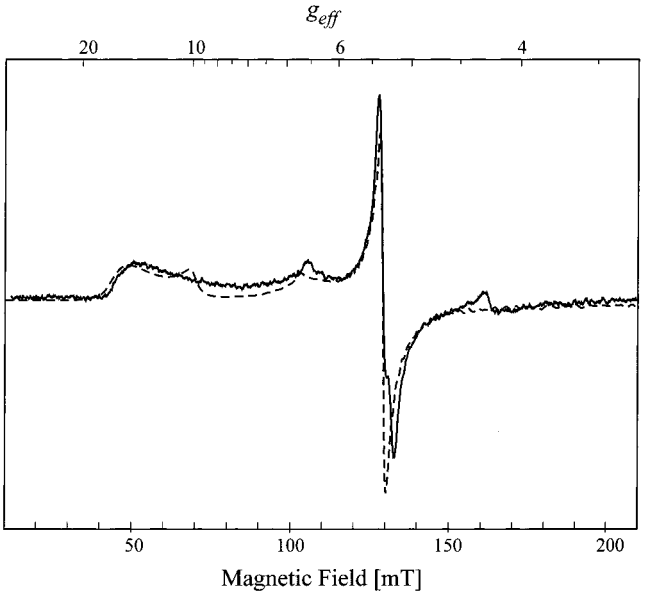

Figure 1. 5 K EPR spectrum of $R2_{mv9/2}$. The spectrum was recorded with the following instrumental settings: microwave frequency, 9.655 GHz; microwave power, 0.2 mW; modulation frequency, 100 kHz; modulation amplitude 1 mT. The dashed line plotted over the data is a theoretical simulation using eq 2 with parameters $S = {}^9/_2$, $D = 1.5$ cm^{-1}, $E/D = 0.05$, and $\sigma_{E/D} = 0.023$.

Results

EPR Spectroscopy. In agreement with the previous finding,[25−27] irradiation of $R2_{met}$ at low temperature yields a species ($[R2_{met}]_{mv1/2}$) that exhibits an $S = {}^1/_2$ axial EPR signal at $\mathbf{g} < 2$ (data not shown), typical of an antiferromagnetically coupled Fe(II)Fe(III) species. Upon annealing at 180 K for 4 min, $[R2_{met}]_{mv1/2}$ converts to $R2_{mv9/2}$ of which the spectrum is shown in Figure 1. The $\mathbf{g} < 2$ signal of $[R2_{met}]_{mv1/2}$ has disappeared, and several resonance signals in the low-field region have appeared: (i) a broad, asymmetric, absorption-like signal at $g \sim 14$, for which the low-field side is considerably steeper than the high-field side, (ii) an absorption like signal at $g = 6.6$, and (iii) an almost isotropic derivative-type signal at $g = 5.4$. These features were previously attributed to the $S = {}^9/_2$ ground multiplet of $R2_{mv9/2}$, and based on a study of temperature dependence, the signal at $g \sim 14$ was asigned to the lowest Kramers doublet of the $S = {}^9/_2$ multiplet, and the signal at $g = 5.4$ to the first excited Kramers doublet.[25] It was noted by Hendrich et al.[25] that the feature at $g = 6.6$ also arises from an excited doublet, but the resonance position does not conform to "the simplistic assumptions of an $S = {}^9/_2$ center." Figure 2 illustrates this point by showing the effective principal g values as a function of E/D for the ground (panel A) and first excited (panel B) doublet calculated according to eq 2. Figure 3 shows the corresponding simulated EPR spectra within a range of E/D values between 0.015 and 0.125. The theoretical spectra for the excited doublet shown in Figure 3B indicate that, although an isotropic derivative-type signal at $g \sim 5.4$ can be simulated with $E/D = 0.055$, the signal at $g = 6.6$ is not reproduced with this parameter. An effective g value of 6.6 (g_y) can be reproduced with an $E/D = 0.075$, but the other two principal g values ($g_x = 6.3$ and $g_z = 5.0$) are different from 5.4, resulting in a rhombic EPR spectrum that is distinct from the spectrum observed for $R2_{mv9/2}$. In other words, the features

(38) Bencini, A.; Gatteschi, D. *Electron paramagnetic resonance of exchange coupled systems*; Springer-Verlag: Berlin, Germany, 1990.
(39) Gaffney, B. J.; Silverstone, H. J. *Biol. Magn. Reson.* **1993**, *13*, 1−57.
(40) Krebs, C. Ph.D. Thesis; Ruhr-Universität Bochum, Germany, 1997.

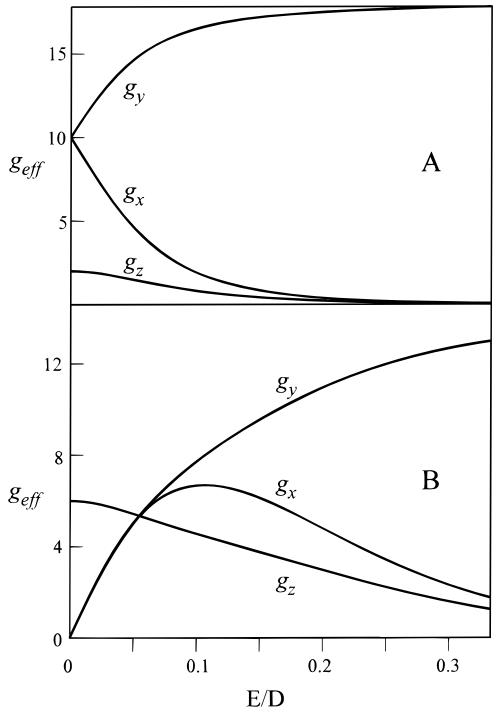

Figure 2. Effective principal g values for the ground (A) and first excited (B) Kramers doublet of an $S = {}^9/_2$ system as functions of E/D. These values are calculated by using eq 2 and assuming $D \gg h\nu$ ($\sim$0.3 cm^{-1} for X-band EPR).

Table 1. Spin Hamiltonian Parameters Used for Simulations of Mössbauer Spectra of $R2_{Mv9/2}$[a]

Fe site	1: Fe^{2+}	2: Fe^{3+}
local spin	2	$^5/_2$
δ (mm/s)	1.25	0.53
ΔE_Q (mm/s)	−2.80	−0.57
η	1.30	−3
$\mathbf{A}/g_n\beta_n$ (T)	−(6.0, 4.8, 9.0)[b]	−(12.3, 12.2, 12.2)
$\mathbf{a}/g_n\beta_n$ (T)	−(13.5, 10.8, 20.3)[b]	−(22.1, 22.0, 22.0)

[a] Spin Hamiltonian parameters used for the electronic ground state of the system are $S = {}^9/_2$, $D = 1.5$ cm^{-1}, $E/D = 0.05$, and $\sigma_{E/D} = 0.023$. [b] The hyperfine tensor of the Fe^{2+} site is rotated with respect to the electronic $\boldsymbol{D}$ tensor by an Euler angle $\beta = 15°$.

observed at $g = 5.4$ and 6.6 cannot be simultaneously simulated with a discrete E/D value. Also, a discrete E/D value cannot reproduce the asymmetric shape of the signal observed at $g \sim 14$. For example, as shown in Figure 2A, even though an effective principal g value of $\sim$14 can be generated for the ground doublet with $E/D = 0.045$, the simulated spectrum (Figure 3A) shows that the signal is symmetric in shape. To reproduce the resonance position and shape of the $g \sim 14$ signal, Hendrich et al.[25] assumed a Gaussian distribution for the rhombicity E/D. Effects of the E/D distribution on the EPR signals originating from the excited doublet, however, were not investigated.

To examine the effects of E/D distribution, we have simulated the EPR spectra for both the ground and first excited Kramers doublets assuming a varied central E/D value and a Gaussian distribution in E/D with a $\sigma_{E/D} = 0.021$.[41] (For these simulations, we have used a D value of 1 cm^{-1}.) The results are plotted in Figure 3 (panels C and D). In comparison with spectra simulated with discrete E/D values (Figure 3, panels A and B), pronounced effects are observed. For the ground doublet, only one prominent EPR feature is observed. Depending on the central E/D value, an absorption-like broad and asymmetric signal is observed between $g = 10$ and 17 (Figure 3C). This signal originates from molecules that have the y-axes of their **g** tensors oriented parallel to the applied magnetic field. Due to the distribution in E/D, there is a spread in g_y. The shape of the observed signal at $g \sim 14$ can then be understood as a result of the weighted superposition of these distributed g_y signals. Signals for the other two principal components, g_x and g_z, are not observed. For the g_x signal, this is because in the conventional derivative representation of an EPR spectrum the g_x signal is of the derivative type (see spectra for the discrete value of E/D shown in Figure 3A), and superposition of a continuous spread of derivative-type signals caused by the E/D distribution results in cancellation of the signals. For the g_z signal, the resonance is outside of the experimental range. Also, superposition of a spread of the g_z signal is expected to generate an extremely broad signal because $\Delta H/\Delta g$ is much larger at the high-field region. For the excited doublet, the distribution in E/D results in two observable features: an absorption like signal at $g = 6.6$ and an isotropic derivative-type signal at $g = 5.4$ (a shoulder at the low-field region of the 6.6 signal is also observed for central E/D values greater than 0.08). Most interestingly, the positions of these two features are in agreement with the experimentally observed g values and are almost independent of the central E/D value. The relative intensities of these two features, on the other hand, are very sensitive to the central E/D value. A central E/D value of 0.05 yields a spectrum that reproduces very well the intensity ratio of the two signals observed for $R2_{mv9/2}$.

On the basis of the above analysis, we conclude that a distribution in E/D may be sufficient to explain all the major EPR features observed for $R2_{mv9/2}$. We have therefore analyzed the EPR data assuming an $S = {}^9/_2$ state with a distribution in E/D and using eq 2. Parameters obtained from the analysis are listed in Table 1 and given in the caption of Figure 1. A theoretical spectrum simulated with these parameters is plotted in Figure 1 as a dashed line. It can be seen that major features of the experimental data are reproduced in the simulated spectrum.

Mössbauer Spectroscopy. Effects of low-temperature (77 K) irradiation and high-temperature annealing on a $R2_{met}$ sample have been monitored by Mössbauer spectroscopy. Before irradiation, the $R2_{met}$ sample exhibits a Mössbauer spectrum (Figure 4A) that consists of two quadrupole doublets ($\Delta E_Q(1) = 1.64$ mm/s and $\delta(1) = 0.54$ mm/s; $\Delta E_Q(2) = 2.41$ mm/s and $\delta(2) = 0.45$ mm/s) indicative of the antiferromagnetically coupled diferric cluster in R2.[6,7,42] Data recorded at strong applied field indicate that the $R2_{met}$ sample also contains an $S = {}^5/_2$ monoferric impurity accounting for (10 ± 2)% of the total iron. The spectrum recorded after irradiation shows that a majority of the clusters ((57 ± 3)% of the total iron) have converted to a paramagnetic species exhibiting magnetic hyperfine features extending from −4 to +5 mm/s (Figure 4B). Spectra recorded at 4.2 K with a 50-mT applied field indicate that this paramagnetic spectral component displays a strong dependence on the orientation of the magnetic field with respect to the direction of the γ-rays, as expected for an $S = {}^1/_2$ system. The hyperfine features and the field orientation dependence of

(41) We are aware of the fact that the assumption of a Gaussian distribution in E/D is too simplistic and cannot reproduce all the fine details observed. However, this approach introduces only one additional parameter ($\sigma_{E/D}$) for spectral simulation. As all major features can be reproduced well by this approach, we did not attempt to further improve the quality of the simulation by introducing further parameters such as considering distributions in D (σ_D) and E (σ_E) independently.

(42) Lynch, J. B.; Juarez-Garcia, C.; Münck, E.; Que, L., Jr. *J. Biol. Chem.* **1989**, *264*, 8091−8096.

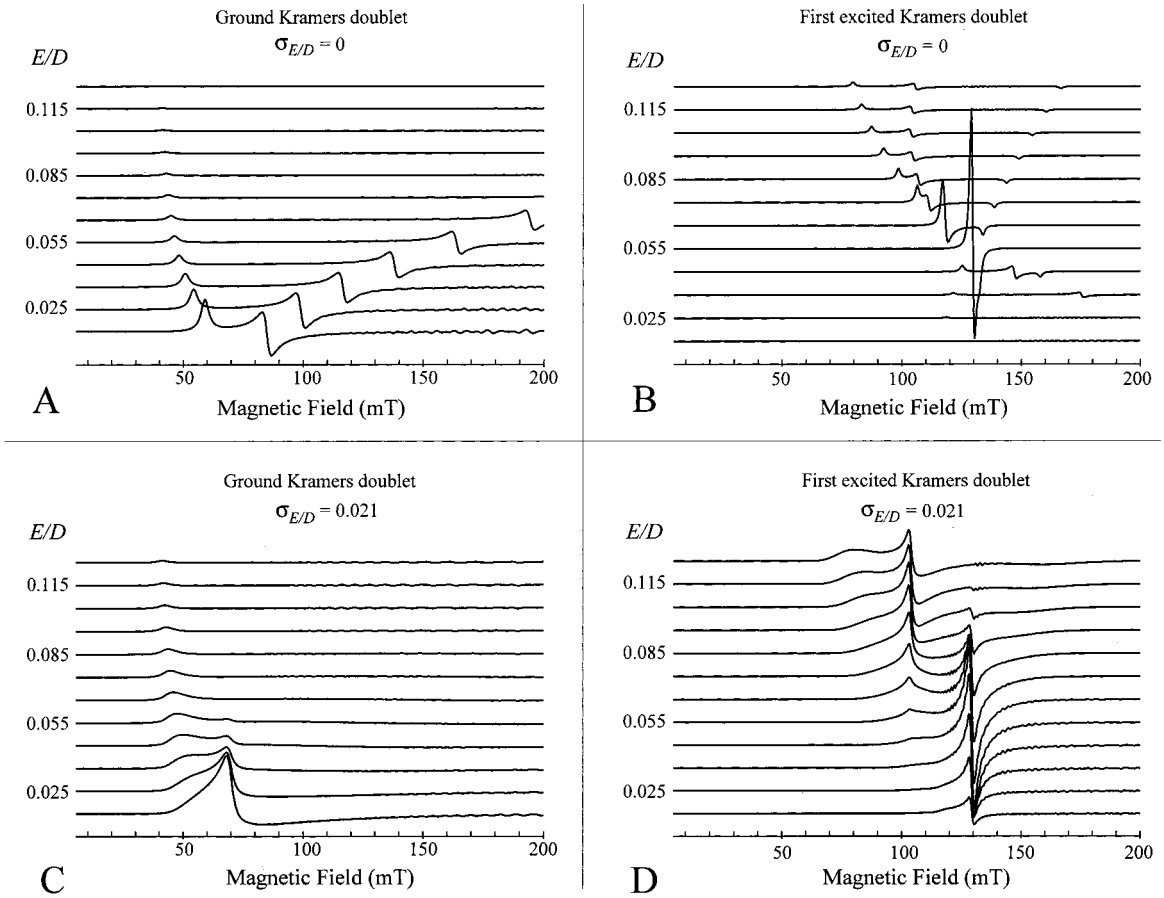

Figure 3. Effects of *E*/*D* distribution on the simulated EPR spectra for the ground (A and C) and first excited (B and D) Kramers doublet of an $S = {}^9/_2$ system. The ordinates in panels C and D show the central *E*/*D* values. These spectra were calculated with $D = 1$ cm^{-1}.

this spectral component are consistent with a valence-localized antiferromagnetically coupled Fe(II)Fe(III) species and the component is assigned to $[R2_{met}]_{mv1/2}$. The irradiation process has also reduced the $S = {}^5/_2$ ferric impurity into an $S = 2$ ferrous impurity, of which the spectrum is a quadrupole doublet at 4.2 K in a 50 mT applied field. The high-energy line of this ferrous quadrupole doublet can be seen in Figure 4B as a resolved peak at +2.7 mm/s (marked by an arrow). A spectrum recorded after the irradiated sample had been annealed at 180 K for 4 min is shown in Figure 4C. The annealing process has no effect on the spectrum of either the diferric cluster or the ferrous impurity. However, the process converts the $S = {}^1/_2$ spectral component to a different paramagnetic spectrum with a much larger magnetic hyperfine splitting (having resonance absorptions between −8 and +8 mm/s). This increase in magnetic splitting is consistent with an $S = {}^1/_2$ to ${}^9/_2$ conversion and the observed spectral change indicates a quantitative conversion of $[R2_{met}]_{mv1/2}$ to $R2_{mv9/2}$. In the following, a detailed Mössbauer characterization of the $R2_{mv9/2}$ is described.

A spectrum of the annealed sample recorded at 120 K (Figure 5A) displays only quadrupole doublets, indicating that the electronic relaxation of $R2_{mv9/2}$ is fast, which results in cancellation of the internal fields at the diiron sites. Removal of the contributions of the diferric cluster (32% of the total iron absorption) and of the ferrous impurity ($\Delta E_Q = 2.70$ mm/s and $\delta = 1.27$ mm/s; 10%) reveals a high-temperature spectrum of $R2_{mv9/2}$ (Figure 5B). Two equal-intensity well-resolved quadrupole doublets are observed. A least-squares fit of the data yields parameters $\Delta E_Q = 2.80 \pm 0.04$ mm/s and $\delta = 1.22 \pm 0.02$ mm/s for doublet 1 and $\Delta E_Q = 0.57 \pm 0.04$ mm/s and $\delta = 0.50 \pm 0.02$ mm/s for doublet 2. These parameters are indicative of high-spin Fe(II) (doublet 1) and high-spin Fe(III) (doublet 2) ions with 5 or 6 O/N ligands. Consequently, this high-temperature spectrum demonstrates unambiguously that $R2_{mv9/2}$ is a valence-localized Fe(II)Fe(III) species.

Figure 6 shows the 4.2 K field-dependent Mössbauer spectra of $R2_{mv9/2}$. These spectra were prepared by removing the contribution of the diamagnetic diferric cluster (32% of total iron absorption) from the raw spectra of the annealed sample. For the 50-mT spectrum (Figure 6A), the contribution from the ferrous impurity ($\Delta E_Q = 2.78$ mm/s and $\delta = 1.31$ mm/s at 4.2 K) has also been removed. It is not possible, however, to remove the ferrous contribution from the strong-field data (1−8 T) because the field dependence of the ferrous impurity is not known. Fortunately, the ferrous impurity is only a minor contribution and should not have a significant effect on the data analysis.

On the basis of the above EPR analysis and a previous EPR study,[25] a distribution in the rhombicity *E*/*D* in $R2_{mv9/2}$ is concluded. This distribution in *E*/*D* is also reflected in the Mössbauer spectrum recorded at 50 mT (Figure 6A). Most notably, the two outermost lines at −7 and +8 mm/s are very broad. The broadening of these peaks is a consequence of a distribution in the spin expectation value caused by the distribution in *E*/*D*. At applied fields stronger than 1 T, however, the effect of *E*/*D* distribution on the Mössbauer spectrum was found to be insignificant. Particularly, sharp and well-resolved peaks are observed for the 4- and 8-T spectra (Figure 6, panels C and D, respectively). This observed field-dependent behavior of the Mössbauer spectra indicates that the electronic Zeeman interaction becomes comparable to the zero-field splitting at a field of about 1 T and dominant at fields larger than 4 T,

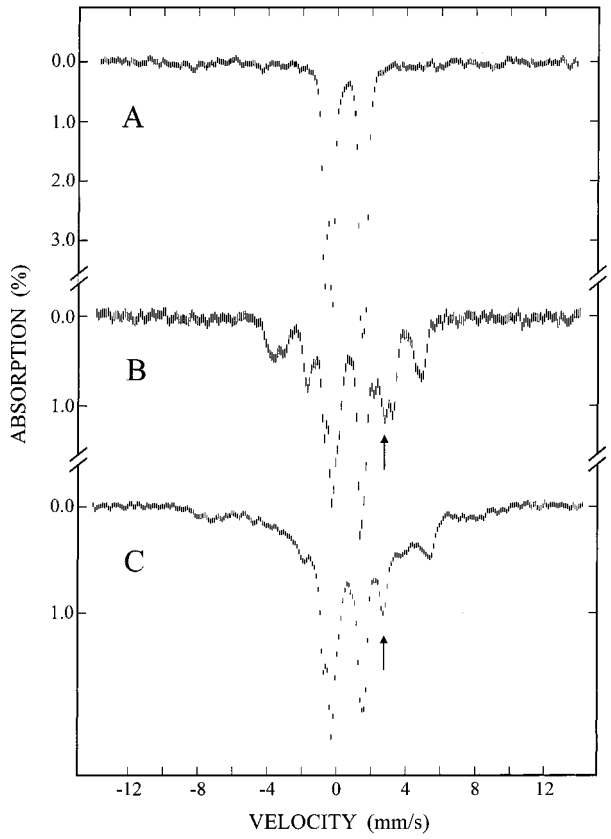

Figure 4. Mössbauer spectra of a $R2_{met}$ sample recorded prior to irradiation (A), after irradiation at 77 K (B), and after annealing the irradiated sample at 180 K (C). The data were recorded at 4.2 K with a magnetic field of 50 mT applied parallel to the γ-rays. The arrows indicate the position of the high-energy line of a quadropule doublet assigned to the ferrous impurity.

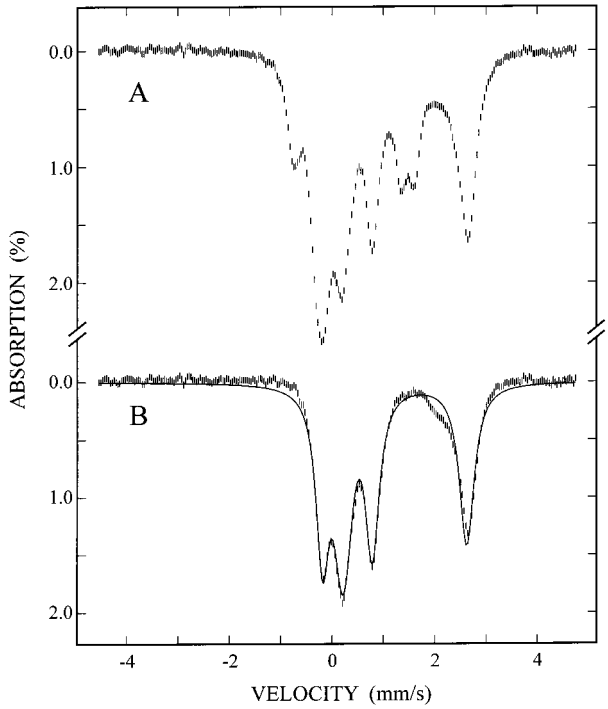

Figure 5. High-temperature Mössbauer spectrum of the annealed sample shown in Figure 4C (A) and the prepared spectrum of $R2_{mv9/2}$ (B). Spectrum B was prepared by removing the contributions of the diferric cluster (32%) and the ferrous impurity (10%) from spectrum A. The data were recorded at 120 K and in the absence of an applied field. The solid line in B is the result of a least-squares fit to the data assuming two equal-intensity quadrupole doublets, parameters of which are given in the text.

suggesting a D value on the order of about 1 cm^{-1} for the $S = {}^9/_2$ ground state. Consequently, analysis of the strong-field spectra (1−8 T) can be performed with a discrete E/D, which is fixed at the central E/D value (0.05) determined from the EPR study.

The analysis of the 4.2 K data has been performed in the slow relaxation limit using eqs 1−3. A pure $S = {}^9/_2$ ground state is assumed in the calculation. Similar to the 120 K spectrum, these 4.2 K spectra (50 mT to 8 T) can also be deconvoluted into two components with parameters (listed in Table 1) typical of high-spin Fe(II) and Fe(III) sites. This observation corroborates the high-temperature finding that $R2_{mv9/2}$ is a valence-localized species. The magnetic hyperfine **A** tensor determined for the Fe(II) site is anisotropic while that of the Fe(III) site is isotropic, as expected for the high-spin states of these oxidation levels. The signs of the **A** tensors are both negative, indicating parallel spin orientation and consistent with the $S = {}^9/_2$ assignment. The magnitudes of the intrinsic **a** tensors are characteristic of O/N ligand environments. Theoretical simulations for $R2_{mv9/2}$ using the parameters listed in Table 1 are plotted over the experimental data in Figure 6. To show that the two components corresponding to the Fe(II) and Fe(III) sites are distinct, simulations for the individual components are plotted in Figure 6 for the 8-T spectrum. As mentioned above, the strong-field spectra (1 to 8 T) have been simulated with a discrete E/D value. For the 50-mT spectrum, however, a distribution in E/D with $\sigma_{E/D} = 0.023$ (as determined from the EPR study) has been used in the simulation. To illustrate the effects of E/D distribution on the weak-field spectrum, a theoretical spectrum simulated with a discrete $E/D = 0.05$ also is plotted above the 50-mT spectrum (Figure 6A). While the assumption of a distribution in E/D allows the broad experimental features to be reproduced well, the theoretical simulation with a discrete E/D value displays sharp absorption peaks.

In an effort to gain information on the effective spin coupling strength (J_{eff}) between the two valence-localized iron sites, we recorded spectra of the annealed sample at high temperatures and in strong fields. Figure 7 shows the 120 (spectrum A) and 60 K (spectrum B) spectrum recorded with a field of 8 T applied parallel to the γ-rays. Contributions from the diferric cluster have been removed for the spectra shown. Analysis of these high-temperature strong-field spectra has been performed using eqs 4−7. Except for J_{eff}, all other parameters in these equations have been determined from the low-temperature Mössbauer and EPR studies presented above. Consequently, only J_{eff} is varied in the analysis of the high-temperature strong-field data and it is found that the major features observed in these spectra may be reproduced with a J_{eff} value between −15 and −10 cm^{-1}. Theoretical simulations using parameters listed in Table 1 and $J_{eff} = -12$ cm^{-1} are plotted over the experimental data in Figure 7. The agreement between the theory and experiment is acceptable in view of the fact that the contributions from the ferrous impurity have not been removed from the data.

Discussion

Low-temperature (77 K) radiolytic reduction of metal clusters in proteins generally generates a reduced cluster trapped in the equilibrium geometry of the oxidized cluster. Annealing at higher temperature may relax the reduced cluster from the constrained oxidized geometry. In the case of $R2_{met}$, low-temperature γ-irradiation yields an antiferromagnetically coupled mixed-valence Fe(II)Fe(III) species, $[R2_{met}]_{mv1/2}$, of which the

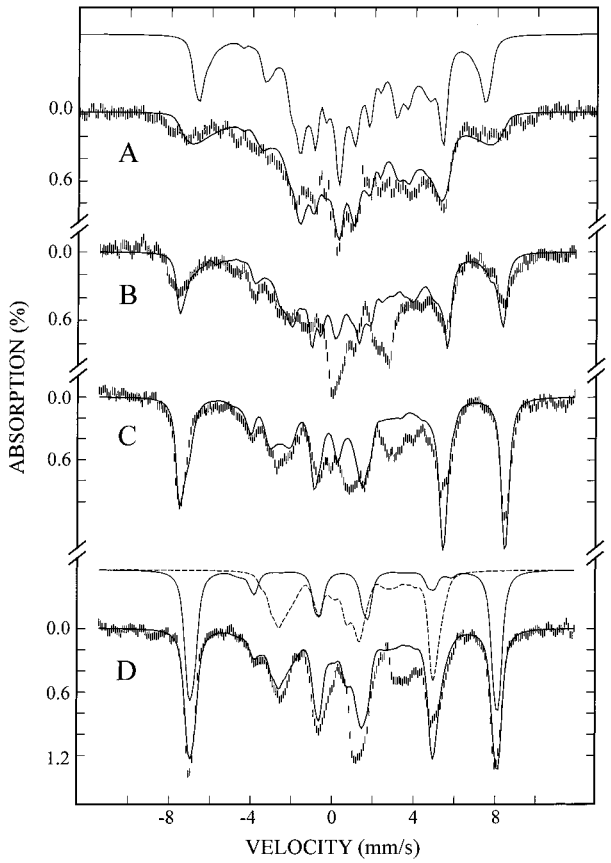

Figure 6. Field-dependent Mössbauer spectra of $R2_{mv9/2}$. The data were recorded at 4.2 K with a field of 50 mT (A), 1 T (B), 4 T (C), and 8 T (D) applied parallel to the γ-rays. Contributions from the diferric cluster have been removed from the raw data. For the 50-mT spectrum, the ferrous impurity contribution also has been removed. The solid lines overlaid with the experimental spectra are theoretical simulations using parameters listed in Table 1. For the 8-T spectrum, individual components corresponding to the ferrous and ferric sites of $R2_{mv9/2}$ are also shown above spectrum D as a dashed and a solid line, respectively. For the simulation of the 50-mT spectrum, a distribution in E/D ($\sigma_{E/D} = 0.023$) has been used. For comparison, a simulation of the 50-mT spectrum with discrete $E/D = 0.05$ is shown above spectrum A as a solid line.

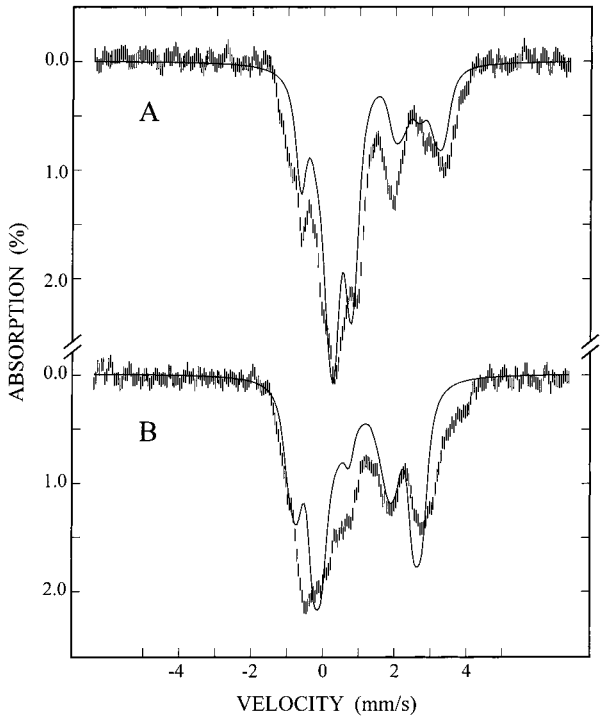

Figure 7. High-temperature strong-field Mössbauer spectra of $R2_{mv9/2}$. The data were recorded in a parallel field of 80 T and at a temperature of 120 (A) or 60 K (B). The contributions from the diferric cluster have been removed from the raw data. The solid lines are theoretical simulations using $J_{eff} = -12$ cm^{-1} and the parameters listed in Table 1.

ground state has the minimum spin value $^1/_2$. With the presence of the bridging oxo group in $R2_{met}$, the antiferromagnetic coupling observed for $[R2_{met}]_{mv1/2}$ is not surprising since the oxo group has been observed to mediate antiferromagnetic coupling for Fe(III)Fe(III) and Fe(II)Fe(III) species.[43−47] Annealing at 180 K converts $[R2_{met}]_{mv1/2}$ to $R2_{mv9/2}$. Low-temperature EPR investigations indicate that the ground state of $R2_{mv9/2}$ has the maximum spin value of $^9/_2$. This observation indicates that the structural relaxation taking place at 180 K causes a switch of the magnetic interaction between the two metal centers from antiferromagnetic to ferromagnetic. We have used Mössbauer spectroscopy to monitor this annealing process and found that the conversion of $[R2_{met}]_{mv1/2}$ to $R2_{mv9/2}$ is stoichiometric and complete within a few minutes. We have also used Mössbauer spectroscopy to investigate in detail the electronic and magnetic properties of $R2_{mv9/2}$. Spectra were recorded over wide ranges of temperatures (4.2−120 K) and applied magnetic fields (0−8 T). The data show unambiguously that $R2_{mv9/2}$ is a valence-localized Fe(II)Fe(III) mixed-valence species; the spectra can be deconvoluted into two components with parameters that are typical for high-spin ferrous and ferric ions with octahedral O/N coordination. The observed field-dependent spectral properties are consistent with the finding by EPR that the magnetic interaction between the two iron sites is ferromagnetic. Furthermore, analysis of the high-temperature strong-field spectra indicates that the effective coupling constant, J_{eff}, is about -12 cm^{-1}.

It has been proposed previously that protonation of the bridging oxo group may be the cause for the change of magnetic interaction observed in the conversion of $[R2_{met}]_{mv1/2}$ to $R2_{mv9/2}$.[26] While protonation of the oxo group may be expected to occur since $R2_{mv9/2}$ is one-electron reduced from $R2_{met}$, evidence accumulated so far indicates that this process alone may not be sufficient to switch the exchange interaction from antiferromagnetic to ferromagnetic. Order-of-mangnitude reduction in the antiferromagnetic exchange interaction caused by protonation of the bridging oxo group is well established for diferric complexes.[43,48] But, ferromagnetic coupling has not been reported for diiron complexes with a single hydoxo bridge. To our knowledge, all Fe(II)Fe(III) species having *one* bridging oxygen group (oxo, hydroxo, phenoxo or alkoxo) known to date display $S = ^1/_2$ ground states, of which many are generated by cryoreduction of diiron proteins and model complexes of known structures.[26−28,44,45,49] Significantly, annealing at $T \geq 220$ K, a cryoreduced mixed-valence mouse R2[28] affords a stable $S =$

(43) Kurtz, D. M., Jr. *Chem. Rev.* **1990**, *90*, 585−606.
(44) Davydov, R. M.; Ménage, S.; Fontecave, M.; Gräslund, A.; Ehrenberg, A. *J. Biol. Inorg. Chem.* **1997**, *2*, 242−255.
(45) Davydov, R. M.; Smieja, J.; Dikanov, S. A.; Zang, Y.; Que, L., Jr.; Bowman, M. K. *J. Biol. Inorg. Chem.* **1999**, *4*, 292−301.
(46) Müller, M.; Bill, E.; Weyhermüller, T.; Wieghardt, K. *Chem. Commun. (Cambridge)* **1997**, 705−706.
(47) Solomon, E. I.; Brunold, T. C.; Davis, M. I.; Kemsley, J. N.; Lee, S.-K.; Lehnert, N.; Neese, F.; Skulan, A. J.; Yang, Y.-S.; Zhou, J. *Chem. Rev.* **2000**, *100*, 235−350.
(48) Armstrong, W. H.; Lippard, S. J. *J. Am. Chem. Soc.* **1984**, *106*, 4632−4633.

$^1/_2$ species that displays an EPR spectrum characteristic of μ-hydroxo Fe(II)Fe(III) centers.[45,50] Also, the only known synthetic mixed-valence Fe(II)Fe(III) complex with a single hydroxo bridge (plus two additional carboxylate bridges) exhibits antiferromagnetic coupling.[50] On the basis of these observations, it is suggested that protonation of the oxo group may not switch the magnetic interaction from antiferromagnetic in $[R2_{met}]_{mv1/2}$ to ferromagnetic in $R2_{mv9/2}$. Additional changes in conformation that promote ferromagnetic interaction are required.

The magnetic interaction between two paramagnetic centers of spins $\mathbf{S}_1$ and $\mathbf{S}_2$ is usually described by the HDvV Hamiltonian $H = J\,\mathbf{S}_1 \cdot \mathbf{S}_2$, in which the exchange coupling constant J is a measure of the strength of the interaction. A negative value of J corresponds to ferromagnetic coupling and yields a parallel alignment for the two spins, $\mathbf{S}_1$ and $\mathbf{S}_2$, in the ground state. A positive J value is associated with antiferromagnetic coupling, which favors an antiparallel alignment of the spins. This treatment is valid for systems in which the valence electrons are localized on the metal sites. For mixed-valence compounds, however, this treatment does not necessarily hold because electrons may delocalize over the two metal centers. An electronic configuration for a mixed-valence binuclear compound with the excess electron localized on one of the metal sites can be described as $d^n d^{n+1}$ or $d^{n+1} d^n$. It has been recognized that mixing of these two configurations (i.e., delocalization) through a resonance interaction splits the states by $\pm B(S + {}^1/_2)$, where S is the system spin and B is the energy parameter describing the strength of this electron-transfer interaction.[30] For a binuclear complex, each possible spin value S occurs twice (due to the presence of the two alternately localized configurations) and the $\pm$ sign indicates that the two states with the same S are split by $2B(S + {}^1/_2)$ by this so-called double exchange interaction. Thus, it can be seen that double exchange interaction is spin dependent: the larger the spin value, the bigger the energy separation. Consequently, the state with the largest system spin S gains the maximum energy by the double exchange interaction. In other words, double exchange tends to stabilize a parallel alignment of the spins of the two metal sites. Generally, whether the compound is valence delocalized or valence localized depends on the relative magnitudes of the double exchange interaction, which tends to delocalize the excess electron, and factors that favor localization of the excess electron. Examples of the latter factors are (1) vibronic coupling, which is a measure of ligand reorganization in response to transfer of the excess electron, and (2) the energy difference between the two localized electronic structures $d^n d^{n+1}$ and $d^{n+1} d^n$ as a consequence of asymmetric ligand environments. Considering only the effect of vibronic coupling, it has been shown that the criterion for delocalization is[30]

$$|B(S + {}^1/_2)| > \lambda^2/k \tag{8}$$

where λ is the vibronic constant that reflects the difference in vibrational energy associated with one of the monomeric iron sites caused by the addition of the excess electron on that site, and k is the force constant for the out-of-phase combination of the breathing motions of the two iron sites. If this criterion is not met, the system is localized and the magnetic interaction between the two localized spins may be described by the HDvV Hamiltonian with an effective coupling constant J_{eff} given by[30]

$$J_{eff} = J - \frac{2B^2}{\lambda^2/k} \tag{9}$$

Equation 9 indicates that effective ferromagnetic interaction ($J_{eff} < 0$) can be observed for localized mixed-valence compounds with antiferromagnetic exchange coupling ($J > 0$), provided that the double exchange interaction overcomes the exchange coupling. In the following, we discuss examples in model compound studies that suggest such a situation may apply to the valence-localized $R2_{mv9/2}$. The examples discussed below also present an alternative possibility in which both double exchange (B) and ferromagnetic exchange ($J < 0$) contribute to the observed ferromagnetic coupling.

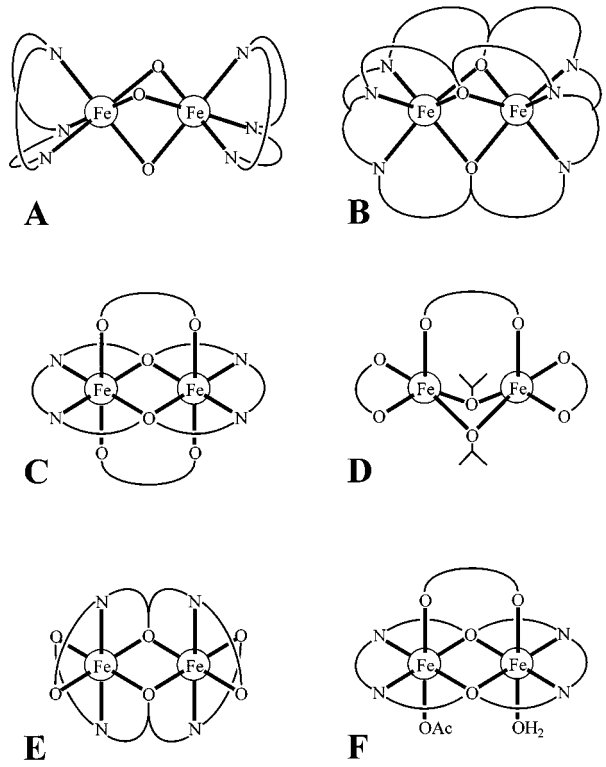

Figure 8. Schematic drawing of the core structures of compounds **A**−**F** listed in Table 2.

In studies on inorganic model complexes, several oxygen-bridged Fe(II)Fe(III) compounds (**A** to **F**) have been found to exhibit $S = {}^9/_2$ ground states.[31−34,40,51−54] A common structural feature shared by these compounds is the presence of (two or three) single-oxygen bridges (Figure 8), resulting in relatively short Fe−Fe distances (Table 2). For compounds **A** to **C**, the valences are delocalized and their double exchange parameters, B, have been determined from the intervalence bands.[33,40,53] A strong correlation between Fe−Fe distance and B is observed; The value of B decreases from 1350 cm^{-1} for compound **A**, which has an Fe−Fe distance of 2.51 Å, to 690 and 944 cm^{-1} respectively for compounds **B** and **C**, which have an Fe−Fe distance of about 2.74 Å. This correlation has been explained

(49) Davydov, A.; Davydov, R.; Gräslund, A.; Lipscomb, J. D.; Andersson, K. K. *J. Biol. Chem.* **1997**, *272*, 7022−7026.
(50) Bossek, U.; Hummel, H.; Weyhermüller, T.; Bill, E.; Wieghardt, K. *Angew. Chem., Int. Ed. Engl.* **1996**, *34*, 2642−5.
(51) Snyder, B. S.; Patterson, G. S.; Abrahamson, A. J.; Holm, R. H. *J. Am. Chem. Soc.* **1989**, *111*, 5214−5223.
(52) Gamelin, D. R.; Bominaar, E. L.; Mathoniere, C.; Kirk, M. L.; Wieghardt, K.; Girerd, J. J.; Solomon, E. I. *Inorg. Chem.* **1996**, *35*, 4323−4335.
(53) Gamelin, D. R.; Bominaar, E. L.; Kirk, M. L.; Wieghardt, K.; Solomon, E. I. *J. Am. Chem. Soc.* **1996**, *118*, 8085−8097.
(54) Dutta, S. K.; Ensling, J.; Werner, R.; Flörke, U.; Haase, W.; Gütlich, P.; Nag, K. *Angew. Chem., Int. Ed. Engl.* **1997**, *36*, 152−155.

Table 2. Selected Physical Properties of Some $S = {}^9/_2$ Mixed-Valence Oxygen-Bridged Fe(II)Fe(III) Compounds

compd[a]	Fe−Fe distance (Å)	valence localization	B (cm^{-1})	J (cm^{-1})	λ^2/k (cm^{-1})	ref
A	2.51	delocalized	1350	<70	2590	32, 52, 53
B	2.745[b]	delocalized	690	90		40
C	2.741	delocalized	943	100		33
D	2.624	delocalized				34
	2.749	localized				34
E	3.081	localized		−17.2[c]	7720	31, 51
	3.116					
F	3.03[d]	localized		−34.0[c]	8620−9010	54

[a] **A**: $[L^1{}_2Fe_2(\mu\text{-}OH)_3]^{2+}$ with L^1 = *N,N′,N″*-trimethyl-1,4,7-triazacyclononane. **B**: $[PhB\{Fe_2dfmp_3\}BPh]$ with H_3dfmp = 2,6-diformyl-4-methylphenoldioxim. **C**: $[L^2Fe_2(\mu\text{-}OAC)_2]^+$ with H_2L^2 = tetraiminodiphenol. **D**: $[L^3{}_3Fe_2(OCHMe_2)_2]$ with L^3 = 2,6-dimesitylbenzoate. **E**: $[L^4Fe_2(\mu\text{-}OAC)(OAC)(H_2O)]^+$ with H_2L^4 = tetraaminodiphenol. **F**: $[Fe_2(salmp)_2]^{1-}$ with salmp = 2-bis(salicylideneamino)methylphenolate(3−). [b] Wieghardt, K., unpublished result. [c] Effective exchange coupling constant J_{eff}. [d] Estimated from an analogue Fe(III)Ni(II) compound.

as a consequence of direct metal−metal orbital interactions that are present in these compounds.[53,55] As the Fe−Fe distance decreases, the inter-metal orbital overlap increases, which in turn promotes double exchange interaction and facilitates electron delocalization.[53] Since the characteristic of valence localization in a mixed-valence compound depends on the strength of double exchange (eq 8), and since B is strongly correlated with the metal−metal distance, a sensitive dependence of valence localization on Fe−Fe distance may be expected.[53] Recently, this sensitivity of valence localization to Fe−Fe distance has been clearly demonstrated in compound **D**, which exists in two conformations with two Fe−Fe distances differing by about 0.12 Å (see Table 2). Compound **D** with the shorter Fe−Fe distance is valence delocalized while compound **D** with the longer Fe−Fe distance displays trapped valence.[34] For $R2_{mv9/2}$, the valences are localized. In other words, the criterion for delocalization (eq 8) is not met. This would limit B to less than a few hundreds of a cm^{-1} ($10B < \lambda^2/k$). Thus, an Fe−Fe distance significantly longer than 2.74 Å is expected for $R2_{mv9/2}$.

For compounds **E** and **F**, the valences are localized.[31,54] Compound **E** crystallizes into two independent molecules in a unit cell.[51] The Fe−Fe distances are 3.08 and 3.11 Å, and the Fe−O−Fe angles are about 96°. The observed ferromagnetic interaction of **E** has been attributed to the presence of an Fe−O−Fe angle close to 90°.[31,51] Such an angle would make orthogonal the magnetic orbitals between the two iron atoms that interact via the p orbitals of the bridging oxygen atoms, and would thus diminish the superexchange pathways and leave the exchange interactions to be dominated by the ferromagnetic potential exchange. Since two-center, two-electron potential exchange integrals are small, the resulting ferromagnetic interaction is expected to be weak (on the order of a few cm^{-1}).[56] With the relatively short Fe−Fe distance in **E**, it is possible that double exchange may also contribute to the observed ferromagnetic coupling ($J_{eff} = -17.2$ cm^{-1}). With the assumption of an exchange interaction of about −10 cm^{-1} (i.e., J = −10 cm^{-1}), a B value of ∼170 cm^{-1} is estimated according to eq 9. Although this estimate is rather arbitrary, the order of magnitude for B appears to be reasonable for an Fe−Fe distance of ∼3.1 Å.[53] Similar arguments may also be applied to compound **F**.

On the basis of the above understanding, it may now be possible to propose a structure for $R2_{mv9/2}$ that is consistent with the observed electronic and magnetic properties. For mixed-valence Fe(II)Fe(III) compounds, a configuration with a single bridging hydroxo group is expected to have weak antiferromagnetic interaction[45,50] and therefore is not a likely structure

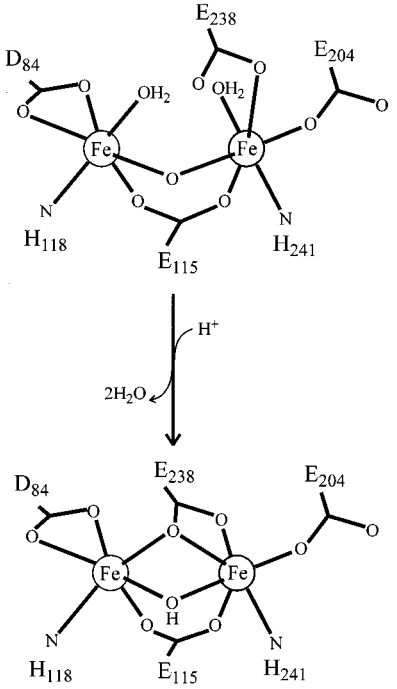

Figure 9. Possible conformational changes taking place at the diiron sites at 180 K, converting $[R2_{met}]_{mv1/2}$ to $R2_{mv9/2}$. The diiron structure of $[R2_{met}]_{mv1/2}$ is assumed to be the same as that of $R2_{met}$.[5]

for $R2_{mv9/2}$. Thus, a configuration with multiple single-oxygen bridges is proposed. However, since $R2_{mv9/2}$ is valence localized, a triply bridged configuration is unlikely because such configuration tends to shorten the Fe−Fe distance to the extent of delocalizing the valences. Consequently, a core structure with two single-oxygen bridges, similar to those of compounds **E** and **F**, is a likely candidate for $R2_{mv9/2}$. It should be noted that the strength of the ferromagnetic coupling, $J_{eff} \sim -12$ cm^{-1}, in $R2_{mv9/2}$ is on the same order of magnitude as those of **E** and **F**. To form such a structure, we suggest that the conformational change taking place upon 180 K annealing may involve shifting of the carboxylate E238 from a monodentate terminal binding mode to a monodentate bridging and chelating mode, in addition to the expected protonation of the bridging oxo group (Figure 9). The proposed binding mode for E238 has been observed in an azide complex of R2[57] and in the R2-D84E mutant,[58] and has been proposed for the Fe(III)Fe(IV) compound **X** of R2.[59]

(55) Saal, C.; Böhm, M. C.; Haase, W. *Inorg. Chim. Acta* **1999**, *291*, 82−90.
(56) Weihe, H.; Güdel, H. U. *Inorg. Chem.* **1997**, *36*, 3632−3639.
(57) Andersson, M. E.; Högbom, M.; Rinaldo-Matthis, A.; Andersson, K. K.; Sjöberg, B. M.; Nordlund, P. *J. Am. Chem. Soc.* **1999**, *121*, 2346−2352.
(58) Voegtli, W. C.; Khidekel, N.; Baldwin, J.; Ley, B. A.; Bollinger, J. M., Jr.; Rosenzweig, A. C. *J. Am. Chem. Soc.* **2000**, *122*, 3255−3261.
(59) Riggs-Gelasco, P. J.; Shu, L.; Chen, S.; Burdi, D.; Huynh, B. H.; Que, L., Jr.; Stubbe, J. *J. Am. Chem. Soc.* **1998**, *120*, 849−860.

Protonation of the oxo group should reduce the antiferromagnetic coupling while shifting of the E238 binding mode should decrease the Fe−Fe distance and the Fe−O−Fe angles, which should reduce further the kinetic exchange, sustain the potential exchange, and increase the double exchange, resulting in the observed ferromagnetic coupling. Obviously, these detailed suggestions require further experimental validation.

Another interesting observation resulting from this study is the effect of zero-field-splitting distribution on EPR spectra. Although the presence of zero-field-splitting distribution in proteins has been recognized by many investigators,[39,60−63] the distribution is generally used to explain only the broadening of EPR line shape through the creation of a distribution in g values. In this study, we show that distributions in zero-field splitting may also have a pronounced effect on the nature of the spectrum and on the apparent g values that are observed. For example, for an $S = {}^9/_2$ system with $D > 0$ a discrete value of $E/D = 0.05$ yields g values at 5.1, 5.0, and 5.4 for the first excited Kramers doublet. These g values are incompatible with the EPR features observed at $g = 6.6$ and 5.4 for $R2_{mv9/2}$. On the other hand, the observed features are properly reproduced if the same $E/D = 0.05$ is the central value, but a distribution in E/D is included in the analysis. A similar situation may apply to the $S = {}^9/_2$ state of a novel Fe−S cluster in fuscoredoxin (also known as the "prismane" protein).[64,65] EPR features at $g = 6.65$ and 5.6, similar to those of $R2_{mv9/2}$, were also detected for fuscoredoxin. These features have been interpreted to reflect two distinct forms of rhombicities with $E/D = 0.061$ for the $g \sim 5.6$ and $E/D = 0.108$ for the $g \sim 6.65$ signal.[66] On the basis of our study, it is likely that these features are results of a distribution in the zero-field splitting. In metalloproteins, $S = {}^9/_2$ systems are rare. However, many proteins contain mononuclear high-spin ferric centers ($S = {}^5/_2$) which display a derivative-type EPR signal at $g = 4.3$ arising from the first excited Kramers doublet. Observation of such a signal is usually attributed to an E/D value of ${}^1/_3$. The common occurrence of such a signal raises the question of whether the E/D value correlates with the local iron environment. On the basis of the current study, a $g \sim 4.3$ signal may arise from superposition of a spread of g values caused by zero-field-splitting distribution (as for the $g = 5.4$ signal observed for $R2_{mv9/2}$) and the central E/D value may not be ${}^1/_3$. EPR spectra of several proteins that contain high-spin ferric ions have been analyzed with E/D distributions.[39,62] Although it was not emphasized in the reports describing the analysis,[62] central E/D values of 0.2 and 0.1, significantly different from ${}^1/_3$, were obtained for several ferric components of these proteins, including transferrin and phenylalanine hydroxylase.

Acknowledgment. We thank Dr. Eckhard Bill for his insightful suggestion of considering E/D distribution in the EPR analysis, Ms. Brenda A. Ley for her assistance in the preparation of the R2 protein, and Dr. Karl Wieghardt for allowing us to quote results prior to publication. This work was supported in part by National Institutes of Health grants GM47295 to B.H.H., GM55365 to JMB, and HL13531 to B.M.H., by the Searle Scholars Program of the Chicago Community Trust, and by the Camille and Henry Dreyfus Foundation (J.M.B.).

JA000317Z

(60) George, G. N.; Prince, R. C.; Bare, R. E. *Inorg. Chem.* **1996**, *35*, 434−438.
(61) Hendrich, M. P.; Debrunner, P. G. *Biophys. J.* **1989**, *56*, 489−506.
(62) Yang, A. S.; Gaffney, B. J. *Biophys. J.* **1987**, *51*, 55−67.
(63) Hearshen, D. O.; Hagen, W. R.; Sands, R. H.; Grande, H. J.; Crespi, H. L.; Gunsalus, I. C.; Dunham, W. R. *J. Magn. Reson.* **1986**, *69*, 440−459.
(64) Tavares, P.; Pereira, A. S.; Krebs, C.; Ravi, N.; Moura, J. J. G.; Moura, I.; Huynh, B. H. *Biochemistry* **1998**, *37*, 2830−2842.
(65) Arendsen, A. F.; Hadden, J.; Card, G.; Mcalpine, A. S.; Bailey, S.; Zaitsev, V.; Duke, E. H. M.; Lindley, P. F.; Kröckel, M.; Trautwein, A. X.; Feiters, M. C.; Charnock, J. M.; Garner, C. D.; Marritt, S. J.; Thomson, A. J.; Kooter, I. M.; Johnson, M. K.; Van Den Berg, W. A. M.; Van Dongen, W. M. A. M.; Hagen, W. R. *J. Biol. Inorg. Chem.* **1998**, *3*, 81−95.
(66) Pierik, A. J.; Hagen, W. R.; Dunham, W. R.; Sands, R. H. *Eur. J. Biochem.* **1992**, *206*, 705−719.